Smart Structures and Systems, *Vol. 34, No. 4 (2024) 229-241*
https://doi.org/10.12989/sss.2024.34.4.229

Seismic performance of steel moment-resisting frame structures equipped with semi-active piezoelectric patches

Fayaz R. Rofooei*[1], Soroush Mosayyebi [1] and Ali Nikkhoo [2]

[1] *Department of Civil Engineering, Sharif University of Technology, 11155-4313 Tehran, Iran*
[2] *Department of Civil Engineering, University of Science and Culture, Tehran, Iran*

(*Received April 1, 2023, Revised June 11, 2024, Accepted November 12, 2024*)

Abstract. The application of piezoelectric patches for semi-active response control of steel special moment-resisting frames (SMRF) subjected to seismic excitations is investigated. Pairs of piezoelectric sheets bonded on the opposite faces of beams and columns are used to apply the required control couples through electric field-induced tensional or compressional strains in the piezoelectric sheets. Also, the modified Bang-Bang control algorithm as a typical control scheme is employed to determine the magnitude of the required control couples. For this purpose, Sap2000 software is utilized for modelling and time history analysis of the considered structural systems, and the MATLAB program is used to calculate the control couples. Furthermore, the open application programming interface (OAPI) codes are prepared for linking the Sap2000 and MATLAB software for online time history analysis of the structural models. The obtained results for a number of steel SMRFs with different numbers of bays and stories indicate that the application of the piezoelectric patches efficiently reduces the structural responses, including story drifts and story absolute accelerations. Also, using a design parameter, "$\boldsymbol{\lambda}$", the best placement of the piezoelectric patches for the structural models is determined, and the responses of the optimally controlled cases are compared with those for the uncontrolled ones.

Keywords: optimal placement; piezoelectric patches; semi-active control; Special Moment Resisting Frame (SMRF); time history analysis

1. Introduction

1.1 Application of piezoelectric materials in structural control

Piezoelectric materials can transform mechanical energy into electrical energy, known as the direct piezoelectric effect, and electrical energy to mechanical energy, recognized as the converse piezoelectric effect. They can be used both as sensors and actuators in semi-active structural control systems. Furthermore, they are light, compact, compatible with different environments, and comparatively easy to use. The piezoelectric materials can be used as semi-active controller by utilizing variable voltage applied to the piezoelectric nodes in a hybrid control system.

Regarding the application of piezoelectric materials in structural control, Rofooei and Nikkhoo (2009) investigated the application of active piezoelectric patches in controlling the dynamic responses of thin rectangular plates under moving masses. Nikkhoo (2014) investigated the behavior of smart thin beams under dynamic loads using piezoelectric actuators. Song and Li (2014) explored the optimal placement of piezoelectric sensors and actuators for vibration control of composite laminated panels. Habib *et al*. (2022) investigated the influence of nonlinear damping on the performance of piezoelectric sensors in both symmetric and asymmetric configurations. Amir *et al*. (2021) explored vibration analysis on sandwich beams with piezoelectric face sheets by the usage of a Proportional-Derivative (PD) controller. Sahin *et al*. (2021) studied the vibration control of smart piezoelectric beams employing an H∞ controller and linear parameter varying (LPV) model. Ju *et al*. (2023) did comprehensive research on piezoelectric materials and sensors' application in structural health monitoring. Lu *et al*. (2020) investigated the application of piezoelectric materials as a base isolation system for reducing the vertical seismic responses of structures. Upadrashta *et al*. (2020) performed on analytical and experimental research on stepped piezoelectric materials for energy harvesting applications. Amini *et al*. (2020) determined optimal placements of piezoelectric pairs (sensors/actuators) in sandwich plates by the usage of an improved genetics algorithm. Aabid *et al*. (2021) reviewed challenges and opportunities in using piezoelectric materials for the control and health monitoring of engineering structures. Trentadu *et al*. (2019) studied the random vibration control of structures via attached piezoelectric strips. Singh *et al*. (2019) studied the influence of surface irregularity on the dynamic response of functionally-graded piezoelectric substrates subjected to a moving load. Jemai and Najar (2018) presented a novel design method for interdigitated electrodes of piezoelectric transducers. Chen *et al*. (2019) studied the fundamentals and applications of piezoelectric materials in sustainable buildings.

*Corresponding author, Ph.D., Professor,
E-mail: rofooei@sharif.edu

ISSN: 1738-1584 (Print), 1738-1991 (Online)

In a state-of-the-art article, Song *et al*. (2006) reviewed the research on civil structures' vibration control using piezoelectric ceramics. Furthermore, Shivashankar and Gopalakrishnan (2020) reviewed the applications of piezoelectric materials for active vibration, noise, and flow control.

This study considers the piezoelectric patches for semi-active control of steel special moment-resisting frames (SMRF) under earthquake excitations. Pairs of piezoelectric sheets that are bonded to the beams and the columns are used to apply the required control couples. Also, the bang-bang control algorithm is employed to compute the magnitude of control couples. Sap2000 software is used to build the structural models, and the MATLAB program is considered to calculate the control actions (couples). The open application programming interface (OAPI) codes are prepared for linking the Sap2000 and MATLAB software. Using a number of structural models, the efficiency of the proposed semi-active control approach in mitigating the seismic response of those models utilizing piezo patches, as well as their optimal placement, is investigated.

1.2 Control algorithm

Among various approaches for active control of structures, the semi-active control mechanisms were given more attention as their application is more feasible in controlling the response of structures under dynamic loadings. Consequently, different control algorithms are developed to operate these control mechanisms. Among the main issues in designing an active control system is the saturation limit on the magnitude of the control forces generated by the actuators. In this regard, the bang-bang control algorithm offered an acceptable performance compared to other control algorithms, such as the linear quadratic regulator (LQR). Lim *et al*. (2003) proposed an adaptive bang-bang control algorithm for the vibration control of structures. Kumar *et al*. (2018) investigated the particle swarm modified quasi bang-bang controller for vibration control. Cheng *et al*. (2010) carried out a theoretical and experimental study on an improved bang-bang control algorithm.

In this study, a modified bang-bang control algorithm introduced by Wu and Soong (1996) is considered just as a typical control algorithm to operate the semi-active piezo patches. Considering a linear 2-dimensional (2-D), n–story shear building structural model, its governing differential equation of motion subjected to a horizontal earthquake ground acceleration of $\ddot{x_g}(t)$ is can be written as Eq. (1).

$$M\ddot{x}(t) + C\dot{x}(t) + Kx(t) = Du(t) + \boldsymbol{m}\,\ddot{x_g}(t) \tag{1}$$

Where $x(t) = \{x_1\, x_2 \ldots x_n\}^T$ is the vector of relative displacement, $u(t) = \{u_1\, u_2 \ldots u_m\}^T$ is the vector of control forces, and $[D]_{n\times m}$ is the location matrix of the controllers. Also, $[M]_{n\times n}$, $[C]_{n\times n}$ and $[K]_{n\times n}$ are the mass, the damping, and the stiffness matrices, respectively. Also, $\boldsymbol{m^T} = -\{m_1\, m_2 .. m_n\}$. The state-space representation of Eq. (1) is shown in Eq. (2).

$$\dot{z}(t) = Az(t) + Bu(t) + E\,\ddot{x}_g(t) \tag{2}$$

In which $z/t)$ is the state-vector, A is the system matrix, B is the location matrix of the controllers, and E is the external disturbance input matrix. These parameters are defined as the followings

$$\{z(t)\}_{2n\times 1} = \begin{Bmatrix}\{x(t)\}_{n\times 1}\\ \{\dot{x}(t)\}_{n\times 1}\end{Bmatrix}$$

$$[A]_{2n\times 2n} = \begin{bmatrix} O_{n\times n} & I_{n\times n} \\ -M_{n\times n}{}^{-1}K_{n\times n} & -M_{n\times n}{}^{-1}C_{n\times n}\end{bmatrix}$$

$$[B]_{2n\times m} = \begin{bmatrix} O_{n\times m} \\ M_{n\times n}{}^{-1}\,D_{n\times m}\end{bmatrix},$$

$$[E]_{2n\times 1} = \begin{bmatrix} O_{n\times 1} \\ M_{n\times n}{}^{-1}\boldsymbol{m}_{n\times 1}\end{bmatrix}$$

The optimal control force in the bang-bang control algorithm is obtained by minimizing the following performance index in Eq. (3).

$$J = \int_0^{t_f} [z^T(t)\, Q\, z(t)]\, dt \tag{3}$$

subject to the following control force constraint in Eq. (4).

$$|u/t)| \le u_{max} \tag{4}$$

The obtained optimal control force in the bang-bang control algorithm is a function of the co-state parameter. Since it is difficult and time-consuming to determine the direction of the control action, a sub-optimal bang-bang control algorithm described by a state-related function was introduced to solve this problem (Wu and Soong 1996, Preumont 1988). In the sub-optimal bang-bang control algorithm, the control force is determined using Lyapunov's direct method, where the control force of the system is obtained by minimizing the time derivative of the Lyapunov function. For a linear system described by Eq. (2), one of the quadratic Lyapunov functions may be selected as Eq. (5).

$$V(t) = z^T(t)Sz(t) \tag{5}$$

Where S is a symmetric positive definite matrix, and it is the solution of the Lyapunov matrix equation given by Eq. (6).

$$A^TS + SA = -Q \tag{6}$$

Since the system matrix, A, is stable and the weighting matrix Q can be selected as a symmetric and positive definite matrix, the matrix S would also be a symmetric positive definite matrix. In this research, the unitary matrix $I_{2n\times 2n}$ was selected as the Q matrix. Therefore, the matrix $[S]_{2n\times 2n}$ can be determined by solving Eq. (6). The control force obtained by minimizing the time derivative of Eq. (5) under the control force constraint given by Eq. (4) can be written as Eq. (7).

$$u(t) = -u_{max}\,.\,sgn\,[B^TSz(t)] \tag{7}$$

Where u_{max} is the maximum control force vector to be generated by the actuators. From Eq. (7), the control force

is expressed in terms of state vector but still has the problem of chattering near the origin of the state-space caused by the high-frequency switching of the control force. Wu and Soong (1996) proposed the modified bang-bang control scheme to overcome this chattering issue. Defining a term that determines the direction of the control force in Eq. (7) as Eq. (8).

$$\{v(t)\}_{m\times 1} = [B^T]_{m\times 2n}\,[S]_{2n\times 2n}\,\{z(t)\}_{m\times 1} \tag{8}$$

The modified bang-bang control algorithm force can now be expressed as Eq. (9) (Wu and Soong 1996)

$$u(t) = -u_{max}\,\frac{\{v(t)\}_{m\times 1}}{|v/t)|} \tag{9}$$

By introducing a new design parameter of ψ and defining η(t) as Eq (10), $|v/t)|$ becomes a function of ψ and η/t) as Eq. (11).

$$\eta(t) = \frac{v^2(t) - \psi^2}{\psi^2} \tag{10}$$

$$|v(t)| = \psi\sqrt{1+\eta(t)} \tag{11}$$

By replacing the expanded expression of $|v(t)|$ in Eq. (11) for $|\eta(t)| < 1$, the control force of u(t) in Eq. (9) can be expressed as Eq. (12).

$$\begin{aligned}\{u(t)\}_{m\times 1} &= -u_{max}\,\frac{\{v(t)\}_{m\times 1}}{|v(t)|}\\ &= -u_{max}\,\frac{\{v(t)\}_{m\times 1}}{\psi\left[1+\frac{1}{2}\eta(t)-\frac{1}{8}\eta^2(t)+\frac{3}{16}\eta^3(t)-\cdots\right]}\end{aligned} \tag{12}$$

By considering proper value for design parameter of ψ and replacing the approximated expression of a discontinuous function of $|v(t)|$ in Eq. (12), the modified bang-bang control algorithm overcomes the undesirable control chattering near the origin of the state-space.

In this study, the seismic responses of three steel SMRF structures with different number of stories and bays are controlled using active piezoelectric patches bonded to the beams and the columns. As already mentioned, the modified bang-bang control algorithm is utilized for seismic response mitigation of the considered structural models under 7 earthquake records as a case study.

2. Structural models and assumptions

The considered structural models include three story-one bay model, five story- two bay model, and seven story-two bay model. The story heights and the bay lengths are equal to 3.5 m and 7 m, respectively, for all structural models. These models were designed for a combination of gravity loads (dead loads and 20 percent of the live loads), and 75 percent of the code suggested base shear force. According to ASCE-7, 2016 code, the structures equipped with supplemental damping are supposed to be designed for a reduced base shear force. Then, the efficiency of the employed control system can be evaluated under earthquake excitations. The considered steel SMRF models are assumed to be located on soil type D (according to ASCE 7-16 code). Fig. 1 presents the designed sections of the structural models. The design of the beams and the columns sections is carried out such that the stress ratios of different structural elements fall within 0.6-0.9.

The vibrational properties of the considered models are presented in Table 1 for the first three modes. For each model, the sum of the effective modal masses of the first three modes is more than 90% of their total mass.

Having designed the considered structural models, time history analyses were performed with and without a semi-active control mechanism using 7 earthquake records. Details of the used strong ground motion records are shown

Table 1 Vibrational characteristics of structural models

Structural models	Period(sec)			Effective modal mass (%)		
	Mode 1	Mode 2	Mode 3	Mode 1	Mode 2	Mode 3
3 Story	1.106	0.406	0.282	91.5	7.6	0.9
5 Story	1.77	0.69	0.396	77.2	14.4	3
7 Story	2.228	0.868	0.499	74.4	15.4	3.4

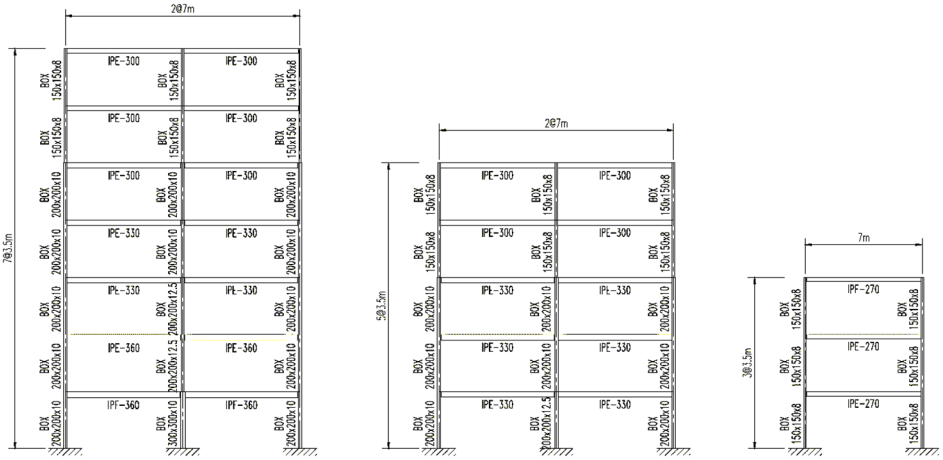

Fig. 1 The designed sections for the 3, 5, and 7 story SMRF structural models

Table 2 Details of strong ground motion records considered in this study

Earthquake ID	Earthquake	Recording station	M	Year	PGA (g)
EQ01	El Centro	El Centro Array	6.9	1940	0.35
EQ02	Northridge	Canyon Country	6.7	1994	0.48
EQ03	El Centro	El Centro Array	6.5	1979	0.38
EQ04	Kobe	Shin-Osaka	6.9	1995	0.24
EQ05	Landers	Coolwater	7.3	1992	0.42
EQ06	Loma Prieta	Gilroy Array	6.9	1989	0.56
EQ07	San Fernando	Hollywood Stor	6.6	1971	0.21

in Table 2. Also, the 5% damped pseudo-accelerations spectra for the considered earthquake records, are illustrated in Fig. 2. All the records are scaled to a PGA of 0.4 g as a measure of design basis earthquake (DBE) intensity.

Furthermore, the following practical assumptions are made for the parametric study.

a) The control forces were applied only to three stories in each controlled structural model.

b) Three approaches for semi-active control of the structural models are considered

- Applying the control couples induced by the active piezoelectric patches to the beams only,
- Applying the control couples induced by the active piezoelectric patches to the columns only,
- Applying the control couples induced by the active piezoelectric patches to both beams and columns.

Therefore, there will be 3 cases for the three-story models, 30 cases for the five-story models, and 105 cases for the seven-story structural models.

c) The control tensional and compressional forces generated by the activated piezoelectric patches that are bonded to the top and bottom flanges of the beams and opposite faces of the column sections produce the pair of control couples as shown in Fig. 3. For numerical analysis purposes, the distributed control couples are replaced with their equivalent concentrated pair of control couples as illustrated in Fig. 3. Assuming linear elastic behavior for the structural models and the piezo materials, the equivalent system should yield the same results as the actual case.

d) The necessary information regarding the dimensions and mechanical properties and practical implementation of the utilized piezoelectric materials are provided here to better demonstrate the feasibility of using the piezoelectric patches in seismic response control of the structural models.

The piezoelectric patches with a length of 1 m are considered to be bonded to the top and bottom flanges of the middle part of the beams (where the maximum positive moments occur) and with a length of 0.5 m on the opposite sides of the columns, close to the beam-column joints (where the negative moments are maximum). Among various types of piezoceramics, the PZT-5A, PZT-5H, and PZT-5J can be selected as having acceptable performance in very high temperatures, ordinary temperatures, and the temperatures in between, respectively. The piezo patches of the type T110-H4NO-2929 with 72.4 mm length, 72.4 mm width, and 0.27 mm thickness made from PZT-5H piezoceramic are considered in this study (https://piezo.com/collections/piezo-sheets-plates). By the side-wise bonding of 14 piezo pieces, a patch with a length of 1013.6 mm can be accommodated on the beams' upper and lower flanges. Similarly, a patch with a length of 506.8 mm can be prepared by using 7 pieces of piezo patches to be bonded on the opposite faces of columns. Furthermore, by bonding 7, 9, and 12 piezo layers, an approximate thickness of 2.1 mm, 2.7 mm, and 3.6 mm can be secured for the proposed patches in 3, 5, and 7-story models, respectively. A schematic view of the proposed piezoelectric patches and the application point of the equivalent couple for the three-story model is presented in Fig. 3.

e) The maximum stress demand in the piezoelectric patches is considered to be less than the yield stress of the PZT-5H piezo materials (around 50% of the yield stress). Wang *et al.* (2019) reported that the yield strength of PZT-5H piezo materials under dynamic loading is approximately 150 MPa. As an example, the upper bound for the induced extensional or compressional forces F_{max} in the utilized PZT-5H piezo materials in the 3-story models can be determined as Eq. (13).

$$F_{max} = \sigma_{max} A = 0.5\sigma_y b t_p \tag{13}$$

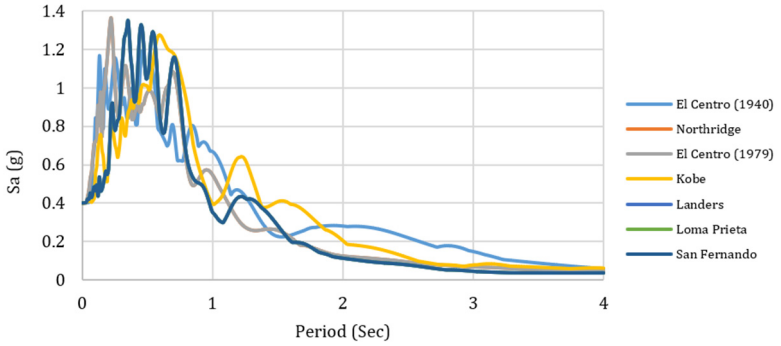

Fig. 2 The pseudo-acceleration spectrums of the selected records

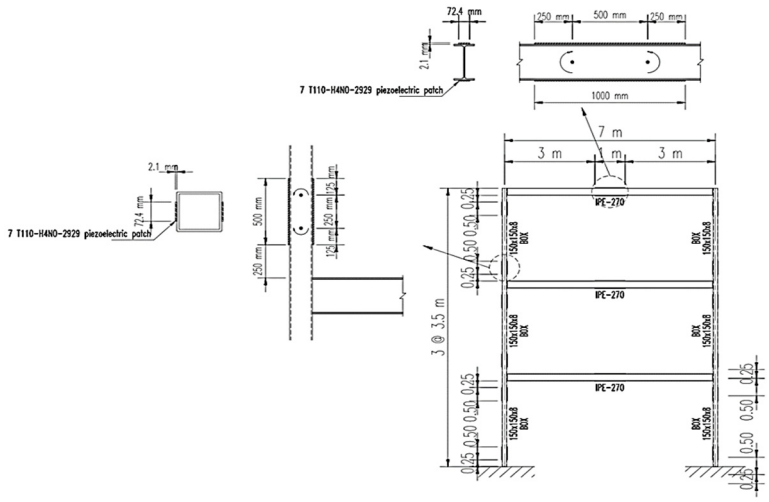

Fig. 3 A schematic view of the utilized piezoelectric patches and their application points of the equivalent couples on the beams and the columns for the three-story structural mode

In which, A, b and t_p are the area, the width and the thickness of the utilized piezo material, respectively. So, the maximum force produced by the upper and lower layers of the piezo patches would be equal to Eq. (14).

$$F_{max} = 0.5 \times 150\, {}^{N}/_{mm^2} \times 72.4 \times 2.1 \cong 11.403kN \quad (14)$$

Multiplying the F_{max} by the distance between the layers of the piezo patches bonded to the beams or the columns, the control pair of couples u (t) is generated. In that respect, Eqs. (15) and (16) can be used to determine the u_{max} for the beams and the columns of the 3-story models, respectively. In which, h is the height of beam section, B is the side dimension of column section, and t_p is the thickness of utilized piezo layers.

$$u_{max,Beams} = F_{max}(h + t_p) = 11.403\ kN \times (270\ mm + 2.1\ mm) \cong\ 3.1\ kN.m \quad (15)$$

$$u_{max,Columns} = F_{max}(B + t_p) = 11.403\ kN \times (150\ mm + 2.1\ mm) \cong\ 1.73\ kN.m \quad (16)$$

Considering the designed sections shown in Fig. 1, the u_{max} values for all the beams and the columns are inserted in Eq. (12). The obtained values of u_{max} for the designed beam and column sections of the structural models are shown in Tables 3 to 5. The determined values for the u_{max} are dependent on the considered performance of the control system. Using higher values for u_{max} will result in smaller response parameters at a higher cost. In Table 5, $u_{max,Columns}$ is determined for the bigger column section, as they are not the same in the first floor.

Also, using a longer length of the piezoelectric patches affects the application point of the control pair of couples. Finally, the maximum required voltage for the considered piezoelectric patch is calculated by assuming linear elastic behavior for the piezoelectric materials as Eq. (17).

$$\varepsilon_{max} = 0.5\varepsilon_y = \frac{0.5\sigma_y}{E_P} = \frac{d_{31}V_{max}}{t_P} \quad (17)$$

Table 3 The maximum couples produced by the piezoelectric patches for the three-story model

Story	$u_{max,Beams}$ (kN.m)	$u_{max,Columns}$ (kN.m)
1, 2 and 3	3.1	1.73

Table 4 The maximum couples produced by the piezoelectric patches for the five-story models

Story	$u_{max,Beams}$ (kN.m)	$u_{max,Columns}$ (kN.m)
1, 2 and 3	4.88	2.97
4 and 5	4.44	2.24

Table 5 The maximum couples produced by the piezoelectric patches for the seven-story models

Story	$u_{max,Beams}$ (kN.m)	$u_{max,Columns}$ (kN.m)
1	7.11	5.93*
2	7.11	3.98
3,4	6.52	3.98
5	5.93	3.98
6,7	5.93	3

In which, ε_y, σ_y , E_P and t_P are the yield strain, yield strength, Young's modulus, and the thickness of the piezo materials, respectively, and d_{31} is the extensional piezoelectric constant. Also, V_{max} is the maximum required voltage. As mentioned before, according to Wang *et al*. (2019), the yield strength of PZT-5H piezoceramics is approximately 150 MPa. Also, the Young's modulus and piezoelectric extension constant of PZT-5H are 50 GPa and 320×10^{-12} m/V, respectively (https://piezo.com/collections/piezo-sheets-plates).
Therefore, using Eq. (16), the V_{max} for any of the utilized piezoelectric materials in the three-story models will be calculated as Eq. (18).

Table 6 The maximum considered voltages for the piezoelectric patches bonded to the beams and columns of the considered models

	$V_{max,Beams}\ (kV)$	$V_{max,Columns}\ (kV)$
3-story models	137.82	68.91
5-story models	177.18	88.59
7-story models	236.25	118.125

$$\frac{0.5 \times 150 \times 10^6\ (Pa)}{50 \times 10^9\ (Pa)} = \frac{320 \times 10^{-12}\ (^m/_V) \times V_{max}}{2.1 \times 10^{-3}\ (m)} \rightarrow V_{max} = 9843.75\ V \cong 9.84\ kV \quad (18)$$

As mentioned before, there are a series of 14 and 7 piezoelectric patches on each of the beams (with a length of 1 m) and columns (with a length of 0.5 m), respectively. Since these patches are connected in series, the maximum required voltage for the performance of piezoelectric patches is equal to 14 × 9.84 ≅ 137.82 kV for beams and 7 × 9.84 ≅ 68.91 kV for columns. Table 6 shows the maximum considered electric voltage for the performance of the piezoelectric patches on beams and columns for the developed structural models.

f) It is also assumed that the piezoelectric patches used for the beams and the columns could produce the required level of control couples without any de-bonding. Furthermore, although insignificant, the time delay in executing the control commands is not considered in this study.

The open application programming interface (OAPI) codes were prepared to link the Sap2000 to MATLAB software for time-history analyses of the prepared models. These codes are employed online, meaning that to determine the structural response at each time step, the previous step's results together with the new ground acceleration input, and the determined control couples (using the previous step's feedback) should be available. Therefore, the online application of the required control forces takes place through the application of the piezoelectric patches. Next, the uncontrolled and controlled structural responses of the models are compared. Moreover, a parametric study is carried out to determine the optimal places on beams and columns to apply the piezoelectric patches. In that regard, a simple yet effective method is suggested to determine the optimal positions for the piezoelectric patches based on the root mean square (RMS) of the response parameters obtained from the time history analyses. It is an efficient measure as it considers the maximum structural responses of all floors subject to any of the earthquake records. The following steps is taken to determine the optimal positions for the piezoelectric patches.

1) For each uncontrolled and controlled model, the maximum drift ratios (%) and maximum absolute accelerations are calculated for all stories of each structural model for each earthquake record.

2) The RMS of the story drift ratios and story absolute accelerations are calculated for each model and for each earthquake record. Specifically, if $d_1, d_2, \dots d_n$ are the story drift ratios for stories "1" to "n" in any structural model, the RMS of drift ratios for that model is calculated according to Eq. (19)

$$d_{RMS} = \sqrt{\frac{{d_1}^2 + {d_2}^2 + \cdots + {d_n}^2}{n}} \quad (19)$$

Moreover, if $a_1, a_2, \dots, a_n$ are the average absolute accelerations for stories "1" to "n" in any structural model, the RMS of the absolute accelerations for that model will be determined as Eq. (20).

$$a_{RMS} = \sqrt{\frac{{a_1}^2 + {a_2}^2 + \cdots + {a_n}^2}{n}} \quad (20)$$

3) For each earthquake record, by dividing the obtained d_{RMS} and a_{RMS} parameters for the controlled models over those of uncontrolled ones, the dimensionless parameters α and β are determined by Eq. (21) and (22), respectively.

$$\alpha = \frac{d_{RMS\ controlled}}{d_{RMS_{uncontrolled}}} \quad (21)$$

$$\beta = \frac{a_{RMS\ controlled}}{a_{RMS_{uncontrolled}}} \quad (22)$$

4) Finally, due to the importance of both story drift ratio (for primary structural elements) and absolute acceleration (for nonstructural components), a sum of these two parameters with equal weighting is considered in this study for determining the optimal positions of the piezoelectric patches as described by Eq. (23) (for each earthquake record)

$$\lambda = 0.5\alpha + 0.5\beta \quad (23)$$

For each structural model, the arrangement of piezoelectric patches with the minimum average λ (over the earthquake records) is considered as the optimal case. The flowchart presented in Fig. 4 briefly explains the different steps to be taken for determining the optimal positions of piezoelectric patches for a given structural model.

3. Numerical results

3.1 Three-story models

For the three-story structural model with different placements of piezoelectric patches (on beams only, on columns only, and on both beams and columns), the application of piezo patches led to a considerable reduction in story drift ratios and absolute accelerations. Table 7 presents the calculated $\boldsymbol{\lambda}$ values for different control cases of the three-story model subjected to the considered

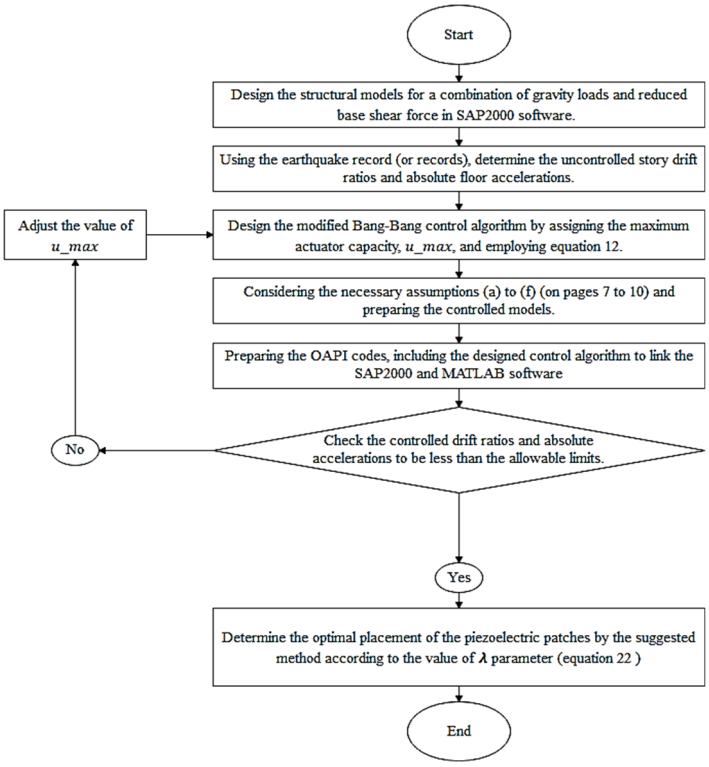

Fig. 4 The proposed procedure for seismic control of steel SMRF models by application of active piezoelectric patches

Table 7 The $\boldsymbol{\lambda}$ values for different control cases of three-story model

Earthquake record ID	Value of λ based on the location of piezoelectric patches		
	Beams only	Columns only	Both beams & Columns
EQ01	0.134	0.145	0.131
EQ02	0.184	0.199	0.18
EQ03	0.145	0.157	0.142
EQ04	0.092	0.099	0.09
EQ05	0.161	0.174	0.157
EQ06	0.214	0.232	0.209
EQ07	0.08	0.087	0.078
Average	0.144	0.156	0.141

earthquake records. Also, Table 7 provides the average of the λ for all earthquake records in each case.

Table 8 shows the average of the maximum drift ratios of different stories for the control cases of three- story model. As Table 8 indicates, the average of maximum uncontrolled drift ratios is much higher than the allowable deign limit of 0.2%, mainly due to using a smaller base shear force in its design. By using piezoelectric patches, the controlled drift ratios become much closer to the allowable limit in all controlled cases.

Table 9 provides the average maximum absolute accelerations of each story for different control cases of three-story model. As expected, the absolute acceleration of upper stories is greater than those for lower stories due to the dominant first mode effect. As Table 9 indicates, in three-story model, the average of maximum uncontrolled absolute accelerations were significantly reduced in all control cases.

Generally, the Tables 7, 8 and 9 indicate that in three-story model, application of piezoelectric patches on beams performed better when compared with those installed on columns. Using patches on both beams and columns will result in the best performance. However, since it does not have a considerable difference with beams, therefore, using piezoelectric patches on beams can be suggested for three-story models.

Fig. 5 depicts the response histories of the first floor's drift ratio and 3rd floor 's absolute acceleration of the three-story model under the El Centro 1940 record (EQ01) are presented as an example. As already mentioned, in case of optimal positions for the piezo patches in three-story structural model, the maximum drift ratio of the model under the EQ01 record were reduced from about 2.2% to 0.3%, and the maximum absolute accelerations were reduced from about 0.6 g to 0.1 g. Therefore, the application of piezo patches resulted in a substantial reduction of seismic responses in three-story model.

3.2 Five-story models

ke three-story model, in all of the considered control cases for five-story structural model, application of the piezo patches led to a significant reduction in story drift ratios and absolute accelerations. Similar to Table 7, Table 10 provides the calculated $\boldsymbol{\lambda}$ values and their average, for

Table 8 The average of maximum drift ratios (%) for three-story model, uncontrolled vs controlled cases

Parameter	The average of maximum drift ratios (%) for each story – 3 story model											
	Story 1				Story 2				Story 3			
	Uncontrolled	Controlled-Beams	Controlled-Columns	Controlled-Both	Uncontrolled	Controlled-Beams	Controlled-Columns	Controlled-Both	Uncontrolled	Controlled-Beams	Controlled-Columns	Controlled-Both
Average of the records	2.350	0.284	0.325	0.28	2.234	0.286	0.305	0.276	1.208	0.207	0.238	0.201

Table 9 The average of maximum absolute acceleration (g) for three-story model, uncontrolled vs controlled cases

Parameter	The average of maximum absolute accelerations (g) for each story – 3 story model											
	Story 1				Story 2				Story 3			
	Uncontrolled	Controlled-Beams	Controlled-Columns	Controlled-Both	Uncontrolled	Controlled-Beams	Controlled-Columns	Controlled-Both	Uncontrolled	Controlled-Beams	Controlled-Columns	Controlled-Both
Average of the records	0.221	0.061	0.07	0.052	0.472	0.057	0.06	0.048	0.623	0.097	0.109	0.093

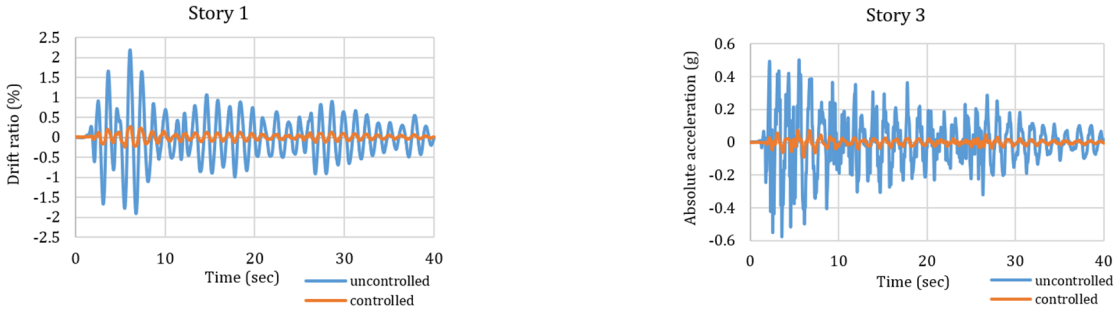

Fig. 5 Uncontrolled vs controlled response time histories of drift ratio (1st floor) and absolute acceleration (3rd floor) under the El Centro 1940 (EQ01) record for three-story model

Table 10 $\boldsymbol{\lambda}$ values for different control cases of five-story model

Earthquake record ID	Value of λ based on the location of piezoelectric patches		
	Beams only	Columns only	Both beams & Columns
EQ01	0.108	0.1	0.064
EQ02	0.148	0.137	0.088
EQ03	0.117	0.109	0.069
EQ04	0.074	0.069	0.044
EQ05	0.13	0.12	0.077
EQ06	0.173	0.16	0.102
EQ07	0.065	0.06	0.038
Average	0.116	0.108	0.069

different control cases of five-story models. As can be seen, the beam and column only cases perform closely while the "both beam-column control case" has the best performance.

Table 11 illustrates the average of maximum drift ratios of each story for different control cases in five-story model. As it shows, the average of maximum uncontrolled drift ratios is much higher than the allowable design limit of 0.2%, for the reason mentioned before. The application of piezoelectric patches (for the optimal position) in five-story model, reduces the drift ratios significantly, satisfying the design drift limit.

Similar to Table 9, the average of maximum absolute accelerations of five-story models are shown in Table 12. As shown in Table 12, the uncontrolled absolute accelerations of different floors are very high (up to 0.7 g). By application of the piezoelectric patches, corresponding values of the model with optimally placed piezo patches was reduced to less than 0.05 g.

Tables 10, 11 and 12 show that in five-story models, the piezoelectric patches placed on columns have a better

Table 11 The average of maximum drift ratios (%) in five-story model - uncontrolled vs controlled cases

Parameter	The average of maximum drift ratios (%) of each story- 5 story model											
	Story 1				Story 2				Story 3			
	Uncontrolled	Controlled-Beams	Controlled-Columns	Controlled-Both	Uncontrolled	Controlled-Beams	Controlled-Columns	Controlled-Both	Uncontrolled	Controlled-Beams	Controlled-Columns	Controlled-Both
Average of the records	4.27	0.407	0.388	0.32	5.243	0.499	0.476	0.392	4.669	0.445	0.425	0.349
Parameter	The average of maximum drift ratios (%) of each story – 5 story models											
	Story 4				Story 5							
	Uncontrolled	Controlled-Beams	Controlled-Columns	Controlled-Both	Uncontrolled	Controlled-Beams	Controlled-Columns	Controlled-Both				
Average of the records	3.335	0.318	0.303	0.25	1.707	0.163	0.155	0.128				

Table 12 The average of maximum absolute accelerations(g) in five-story model - uncontrolled vs controlled

Parameter	The average of maximum drift ratios (%) of each story- 5 story model											
	Story 1				Story 2				Story 3			
	Uncontrolled	Controlled-Beams	Controlled-Columns	Controlled-Both	Uncontrolled	Controlled-Beams	Controlled-Columns	Controlled-Both	Uncontrolled	Controlled-Beams	Controlled-Columns	Controlled-Both
Average of the records	0.187	0.032	0.03	0.024	0.468	0.027	0.026	0.022	0.718	0.038	0.033	0.026
Parameter	The average of maximum drift ratios (%) of each story – 5 story models											
	Story 4				Story 5							
	Uncontrolled	Controlled-Beams	Controlled-Columns	Controlled-Both	Uncontrolled	Controlled-Beams	Controlled-Columns	Controlled-Both				
Average of the records	0.895	0.052	0.046	0.038	0.986	0.059	0.056	0.044				

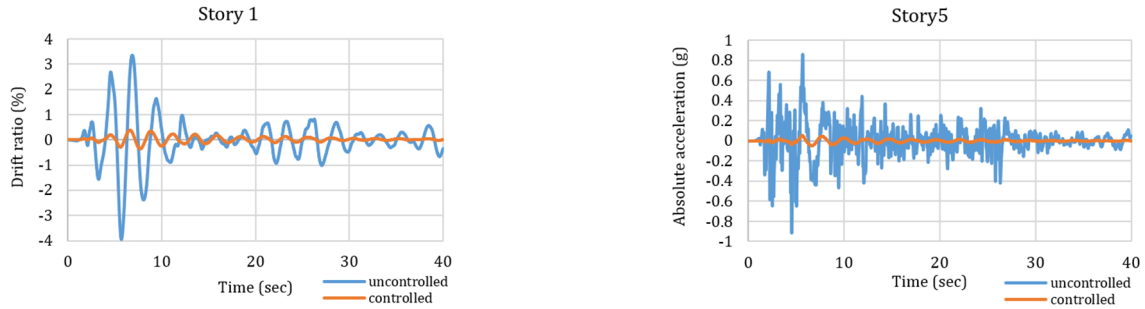

Fig. 6 Uncontrolled vs controlled response time histories of drift ratio (1st floor) and absolute acceleration (5th floor) under the El Centro 1940 (EQ01) record – 5 story model

performance than the beams which could be attributed to the increasing effect of the bending behavior in taller models. Using patches on both beams and columns will again result in a better performance with respect to the case with columns only. Therefore, piezoelectric patches on beams and columns and/or both are recommended choice for five-story model.

As an example, and for the reason mentioned before, the response histories of the drift ratio of the 1st floor and the absolute acceleration of the 5th floor in five-story model

under the El Centro 1940 record (EQ01) are presented in Fig. 6. As Fig. 6 shows, using piezo patches in the five-story structural model for the case of optimally placed piezo patches, reduce the maximum drift ratios from about 4% to less than 0.3%. Also, the maximum absolute accelerations were reduced from about 0.9 g to 0.04 g. Therefore, the usage of semi-active piezo patches leads to a substantial reduction of the seismic responses for 5-story model.

3.3 Seven-story models

Like previous cases, in all of the considered control cases for the seven-story structural model, the application of the semi-active piezo patches resulted in a considerable reduction in story drift ratios and absolute accelerations. Similar to Tables 7 and 10, Table 13 provides the calculated $\boldsymbol{\lambda}$ values and their average, for different control cases for seven-story model.

Table 13 $\boldsymbol{\lambda}$ values for different control cases of the seven-story model

Earthquake record ID	Value of λ based on the location of piezoelectric patches		
	Beams only	Columns only	Both beams & Columns
EQ01	0.095	0.052	0.047
EQ02	0.13	0.071	0.064
EQ03	0.103	0.056	0.051
EQ04	0.065	0.036	0.032
EQ05	0.114	0.062	0.056
EQ06	0.152	0.083	0.075
EQ07	0.057	0.031	0.028
Average	0.102	0.056	0.05

Table 14 indicates the average of the maximum drift ratios for each story for different control cases of seven-story model. As shown in Table 14, and similar to previous cases, the averages of maximum uncontrolled drift ratios (for all earthquake records) are much higher than the allowable design drift limit of 0.2%. The controlled drift ratios become closer to the allowable design limit by using the semi-active piezoelectric patches.

The results shown in Table 15 for optimally placed piezo patches are similar to those for the three and five-story models. The averages of maximum uncontrolled absolute accelerations were up to almost 0.9 g in seven-story model. By application of piezoelectric patches, the corresponding controlled absolute accelerations were reduced to less than 0.1 g. Finally, Tables 13, 14 and 15 demonstrate that like 5-story model, the piezoelectric patches on columns function better than the case for the beams, due to the dominant effect of flexural behavior in seven-story model. Also, as expected using patches on both beams and columns will result in a better performance. However, it does not have a considerable difference with the case of columns only. Therefore, piezoelectric patches on columns yield the best results for seven-story models.

Like previous cases, and for the reason mentioned before, the drift ratio time history of the 1st floor and the

Table 14 The average of maximum drift ratios (%) in seven-story model - uncontrolled vs controlled

Parameter	The average of maximum drift ratios (%) of each story – 7 story model											
	Story 1				Story 2				Story 3			
	Uncontrolled	Controlled-Beams	Controlled-Columns	Controlled-Both	Uncontrolled	Controlled-Beams	Controlled-Columns	Controlled-Both	Uncontrolled	Controlled-Beams	Controlled-Columns	Controlled-Both
Average of the records	3.368	0.916	0.223	0.183	4.279	1.164	0.283	0.233	4.264	1.159	0.282	0.232
Parameter	The average of maximum drift ratios (%) of each story – 7 story model											
	Story 4				Story 5				Story 6			
	Uncontrolled	Controlled-Beams	Controlled-Columns	Controlled-Both	Uncontrolled	Controlled-Beams	Controlled-Columns	Controlled-Both	Uncontrolled	Controlled-Beams	Controlled-Columns	Controlled-Both
Average of the records	4.876	1.326	0.323	0.265	3.977	1.082	0.263	0.216	2.753	0.749	0.182	0.15
Parameter	The average of maximum drift ratios (%) of each story – 7 story model											
	Story 7											
	Uncontrolled	Controlled-Beams	Controlled-Columns	Controlled-Both								
Average of the records	1.404	0.381	0.093	0.077								

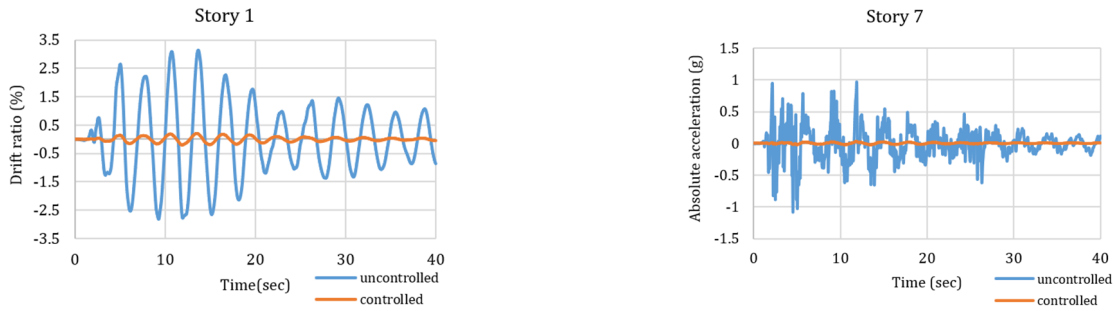

Fig. 7 Uncontrolled vs controlled response time histories of drift ratio (1st floor) and absolute acceleration (7th floor) under the El Centro 1940 (EQ01) record – 7 story model

Table 15 The average of maximum absolute accelerations (g) in seven-story model - uncontrolled vs controlled

Parameter	The average of maximum drift ratios (%) of each story – 7 story model											
	Story 1				Story 2				Story 3			
	Uncontrolled	Controlled-Beams	Controlled-Columns	Controlled-Both	Uncontrolled	Controlled-Beams	Controlled-Columns	Controlled-Both	Uncontrolled	Controlled-Beams	Controlled-Columns	Controlled-Both
Average of the records	0.115	0.03	0.028	0.025	0.301	0.037	0.022	0.019	0.485	0.052	0.018	0.016
Parameter	The average of maximum drift ratios (%) of each story – 7 story model											
	Story 4				Story 5				Story 6			
	Uncontrolled	Controlled-Beams	Controlled-Columns	Controlled-Both	Uncontrolled	Controlled-Beams	Controlled-Columns	Controlled-Both	Uncontrolled	Controlled-Beams	Controlled-Columns	Controlled-Both
Average of the records	0.697	0.068	0.018	0.014	0.87	0.084	0.025	0.018	0.988	0.096	0.032	0.024
Parameter	The average of maximum drift ratios (%) of each story – 7 story model											
	Story 7											
	Uncontrolled	Controlled-Beams	Controlled-Columns	Controlled-Both								
Average of the records	1.05	0.102	0.037	0.027								

absolute acceleration time history of the 7th floor due to the El Centro 1940 record (EQ01) are presented in Fig. 7. As it is shown in Fig. 7 and similar to the three and five-story models, using piezoelectric patches in 7 story structural model led the average of maximum drift ratio to be reduced from about 3% to 0.2%. furthermore, the average of maximum absolute accelerations was reduced from about 1 g to 0.05 g.

4. Conclusions

This study explores the use of the piezoelectric patches for semi-active control of the steel special moment-resisting frame (SMRF) structures subject to earthquake excitation. In this respect, three SMRF models with different numbers of stories and bays are designed for a combination of gravity loads and reduced base shear forces. Using Sap2000 software and considering seven earthquake records, the uncontrolled seismic responses, including story drift ratios and floor absolute accelerations, were determined. As expected, the maximum uncontrolled story drift ratios were much higher than the allowable limit of 0.2% (according to ASCE 7-16 code), and the maximum uncontrolled absolute accelerations were significantly high. In order to reduce the seismic responses, piezoelectric patches were employed as a semi-active control mechanism bonded to the middle of the beams and two ends of the columns of different floors. The distributed control actions produced by the bonded piezoelectric patches are replaced with their equivalent concentrated couples applied to the beams and the columns. Also, the modified bang-bang control algorithm was used through online OAPI codes to link the Sap2000 and MATLAB software. As mentioned, choosing this control

algorithm was optional, and the proposed procedure could perform with any other control algorithm. After performing the time history analyses, the controlled response parameters were calculated. Then, defining a performance parameter, $\boldsymbol{\lambda}$, the optimal placements of the piezoelectric patches were determined for each structural model by comparing the uncontrolled and controlled models' maximum responses (drift ratio and absolute acceleration). The following observations could be made regarding the efficiency of the piezoelectric patches in mitigating the seismic response of the considered models:

1. The seismic performance of the SMRF models under the seven considered earthquake records was improved significantly by using piezoelectric patches. The average of maximum story drift ratios, and floor absolute accelerations were reduced drastically in all cases.
2. In some cases, the controlled structural models' maximum drift ratios were slightly higher than the allowable limit of 0.2%. Nevertheless, the performance of the proposed control scheme could be adjusted depending on the size and distribution of the used piezoelectric patches.
3. The optimal placements of piezoelectric patches were determined numerically by examining the proposed $\boldsymbol{\lambda}$ parameter for all structural models. According to the results of this study, in 3-story structural models, using piezoelectric patches on beams performs more efficiently than the columns. In 5 and 7-story structural models, using piezoelectric patches on columns works better than beams due to the higher contribution of flexural behavior in the overall response of taller models. Similarly, piezoelectric patches on beams perform better for shorter buildings with dominant shear behavior. As expected, application of the piezoelectric patches on both beams and columns leads to better results in all cases.
4. The obtained results are directly dependent on the magnitude of u_{max}. The higher u_{max} will result in a larger reduction of the response parameters at a higher cost.

References

Aabid, A., Parveez, B., Raheman, M.A., Ibrahim, Y.E., Anjum, A., Hrairi, M., Parveen, N. and Mohammed Zayan, J. (2021), "A review of piezoelectric material-based structural control and health monitoring techniques for engineering structures: Challenges and opportunities", In: *Actuators*, Vol. 10, No. 5, p. 101. https://doi.org/10.3390/act10050101

Amini, A., Mohammadimehr, M. and Faraji, A. (2020), "Optimal placement of piezoelectric actuator/senor patches pair in sandwich plate by improved genetic algorithm", *Smart Struct. Syst., Int. J.*, **26**(6), 721-733. https://doi.org/10.12989/sss.2020.26.6.721

Amir, S., Soleimani-Javid, Z. and Maraghi, Z.K. (2021), "Vibration analysis of sandwich beam with honeycomb core and piezoelectric facesheets affected by PD controller", *Smart Struct. Syst., Int. J.*, **28**(2), 195-212. https://doi.org/10.12989/sss.2021.28.2.195

ASCE 7-16 standard: Minimum Design Loads and Associated Criteria for Buildings and Other Structures.

Chen, J., Qiu, Q., Han, Y. and Lau, D. (2019), "Piezoelectric materials for sustainable building structures: Fundamentals and applications", *Renew. Sustain. Energy Rev.*, **101**, 14-25. https://doi.org/10.1016/j.rser.2018.09.038

Cheng, Z., Yu, J. and Wang, X. (2010), "Theoretical and experimental study on an improved Bang-Bang control algorithm", *J. Vib. Shock.*, **29**(2), 60-63. http://jvs.sjtu.edu.cn/CN/abstract/article_1122.shtml

Habib, G., Fainshtein, E., Wolf, K.D. and Gottlieb, O. (2022), "The influence of nonlinear damping on the response of a piezoelectric cantilever sensor in a symmetric or asymmetric configuration", *Smart Struct. Syst., Int. J.*, **30**(3), 239-243. https://doi.org/10.12989/sss.2022.30.3.239

https://piezo.com/collections/piezo-sheets-plates

Jemai, A. and Najar, F. (2018), "Novel design of interdigitated electrodes for piezoelectric transducers", *Smart Struct. Syst., Int. J.*, **22**(4), 369-382. https://doi.org/10.12989/sss.2018.22.4.369

Ju, M., Dou, Z., Li, J.W., Qiu, X., Shen, B., Zhang, D., Yao, F.Z., Gong, W. and Wang, K. (2023), "Piezoelectric materials and sensors for structural health monitoring: fundamental aspects, current status, and future perspectives", *Sensors*, **23**(1), 543. https://doi.org/10.3390/s23010543

Kumar, G., Kumar, A. and Jakka, R.S. (2018), "The particle swarm modified quasi bang-bang controller for seismic vibration control", *Ocean Eng.*, **166**, 105-116. https://doi.org/10.1016/j.oceaneng.2018.08.002

Lim, C.W., Chung, T.Y. and Moon, S.J. (2003), "Adaptive bang–bang control for the vibration control of structures under earthquakes", *Earthq. Eng. Struct. Dyn.*, **32**(13), 1977-1994. https://doi.org/10.1002/eqe.310

Lu, L.Y., Lin, G.L., Chen, Y.S. and Hsiao, K.A. (2020), "Vertical equipment isolation using piezoelectric inertial-type isolation system", *Smart Struct. Syst., Int. J.*, **26**(2), 195-211. https://doi.org/10.12989/sss.2020.26.2.195

Nikkhoo, A. (2014), "Investigating the behavior of smart thin beams with piezoelectric actuators under dynamic loads", *Mech. Syst. Signal Process.*, **45**(2), 513-530. https://doi.org/10.1016/j.ymssp.2013.11.003

Preumont, A. (1988), "Spillover alleviation for nonlinear active control of vibration", *J. Guidance, Control, Dyn.*, **11**(2), 124-130. https://doi.org/10.2514/3.20281

Rofooei, F.R. and Nikkhoo, A. (2009), "Application of active piezoelectric patches in controlling the dynamic response of a thin rectangular plate under a moving mass", *Int. J. Solids Struct.*, **46**(11-12), 2429-2443. https://doi.org/10.1016/j.ijsolstr.2009.01.034

Sahin, M., Turan, A. and Onat, C. (2021), "Vibration control of a smart piezo beam via gain scheduling H∞ controller based on LPV model", *Smart Struct. Syst., Int. J.*, **27**(1), 61-71. https://doi.org/10.12989/sss.2021.27.1.061

Shivashankar, P. and Gopalakrishnan, S.J.S.M. (2020), "Review on the use of piezoelectric materials for active vibration, noise, and flow control", *Smart Mater. Struct.*, **29**(5), p. 053001. https://doi.org/10.1088/1361-665X/ab7541

Singh, A.K., Negi, A. and Koley, S. (2019), "Influence of surface irregularity on dynamic response induced due to a moving load on functionally graded piezoelectric material substrate", *Smart Struct. Syst., Int. J.*, **23**(1), 31-44. https://doi.org/10.12989/sss.2019.23.1.031

Song, Z.G. and Li, F.M. (2014), "Optimal locations of piezoelectric actuators and sensors for supersonic flutter control of composite laminated panels", *J. Vib. Control*, **20**(14), 2118-2132. https://doi.org/10.1177%2F1077546313480538

Song, G., Sethi, V. and Li, H.N. (2006), "Vibration control of civil structures using piezoceramic smart materials: A review", *Eng.*

Struct., **28**(11), 1513-1524. https://doi.org/10.1016/j.engstruct.2006.02.002

Trentadu, F., Quaranta, G., Maruccio, C. and Marano, G.C. (2019), "Energy harvesting from piezoelectric strips attached to systems under random vibrations", *Smart Struct*. *Syst*., *Int*. *J*., **24**(3), 333-343. https://doi.org/10.12989/sss.2019.24.3.333

Upadrashta, D., Xiangyang, L. and Yaowen, Y. (2020), "Analytical and experimental investigation of stepped piezoelectric energy harvester", *Smart Struct*. *Syst*., *Int*. *J*., **26**(6), 681-692. https://doi.org/10.12989/sss.2020.26.6.681

Wang, R., Tang, E. and Yang, G. (2019), "Dynamic Piezoelectric Properties of PZT-5H Under Shock Compression", *physica status solidi* /*a*), **216**(6), p. 1800859. https://doi.org/10.1002/pssa.20180085

Wu, Z. and Soong, T.T. (1996), "Modified bang-bang control law for structural control implementation", *J. Eng*. *Mech*., **122**(8), 771-777. https://doi.org/10.1061/(ASCE)0733-9399(1996)122:8(771)